Electronic Supplementary Material (ESI) for RSC Advances.


# Supporting information

## A new approach for ultra-high adsorption of cationic methylene blue in a Zr-sulfonic-based metal-organic framework

Thinh T. M. Bui,[a] Linh T. Nguyen,[a] Nha P. H. Pham,[a] Cuong C. Tran,[a] Loc T. Nguyen,[a] Tien A. Nguyen,[a] Hung N. Nguyen[a] and My V. Nguyen*[a]

[a] Falcuty of Chemistry, Ho Chi Minh City University of Education, Ho Chi Minh City 700000, Vietnam

*To whom correspondence should be addressed: *mynv@hcmue.edu.vn*

## Table of Contents

## **Section S1.** Materials and Analytical Techniques

**Starting Materials and General Procedures.** Zirconium chloride octahydrate ($ZrOCl_2 \cdot 8H_2O$, 99%), 2,6-napthalenedicarboxylic acid ($H_2NDC$, 98%), oleum (25%), N,N-dimethylformamide (DMF, 98%), sulfuric acid ($H_2SO_4$, 98%), hydrochloric acid (HCl, 37%), formic acid (HCOOH, 96%), methylene blue (MB, 98%), Methanol ($CH_3OH$, 99%) were obtained from Merk and Prolabo chemical. All other chemicals were purchased from local vendors and all chemicals were used without further purification.

Thermal gravimetric analysis (TGA-DSC) was performed on a LabSys Evo thermal analysis system under dry air flow. Fourier transform infrared spectroscopy (FT-IR) measurements were carried out using a Jasco spectrometer with the Attenuated Total Reflectance (ATR) sampling method used. Powder X-ray data presented herein were a Bruker D8 Advance employing Ni filtered Cu $K_\alpha$ ($\lambda$ = 1.54718 Å). The system was equipped with an anti-scattering shield that prevents incident diffusion radiation from hitting the detector. $N_2$ adsorption measurement were conducted using a Micromeritics 3Flex Surface Characterization Analyzer. UV-Vis spectra were analysed on a UV-Vis spectrometer with model: Lamda 25.

**Synthesis of DUT-52.** $ZrCl_4$ (0.115 g, 0.493 mmol) and DMF (10 mL) were ultrasonically dissolved for 5 min in a 20 mL Pyrex vial. Then, 2,6-naphthalenedicarboxylic acid (0.108 g), and $CH_3COOH$ (1.5 mL) were added to the above mixture and ultrasonicated in 15 min. The mixture was heated at 120 $^oC$ for 24h. Subsequently, the sample was washed with DMF for 3 days (6 mL per day) and exchanged with MeOH for 3 days (7 mL per day). After that, the material was centrifugated, dried and activated under vacuum at 80 $^oC$ for 10h to acquire a pure DUT-52.

**Section S2.** The modelling structure of VNU-23 and MB

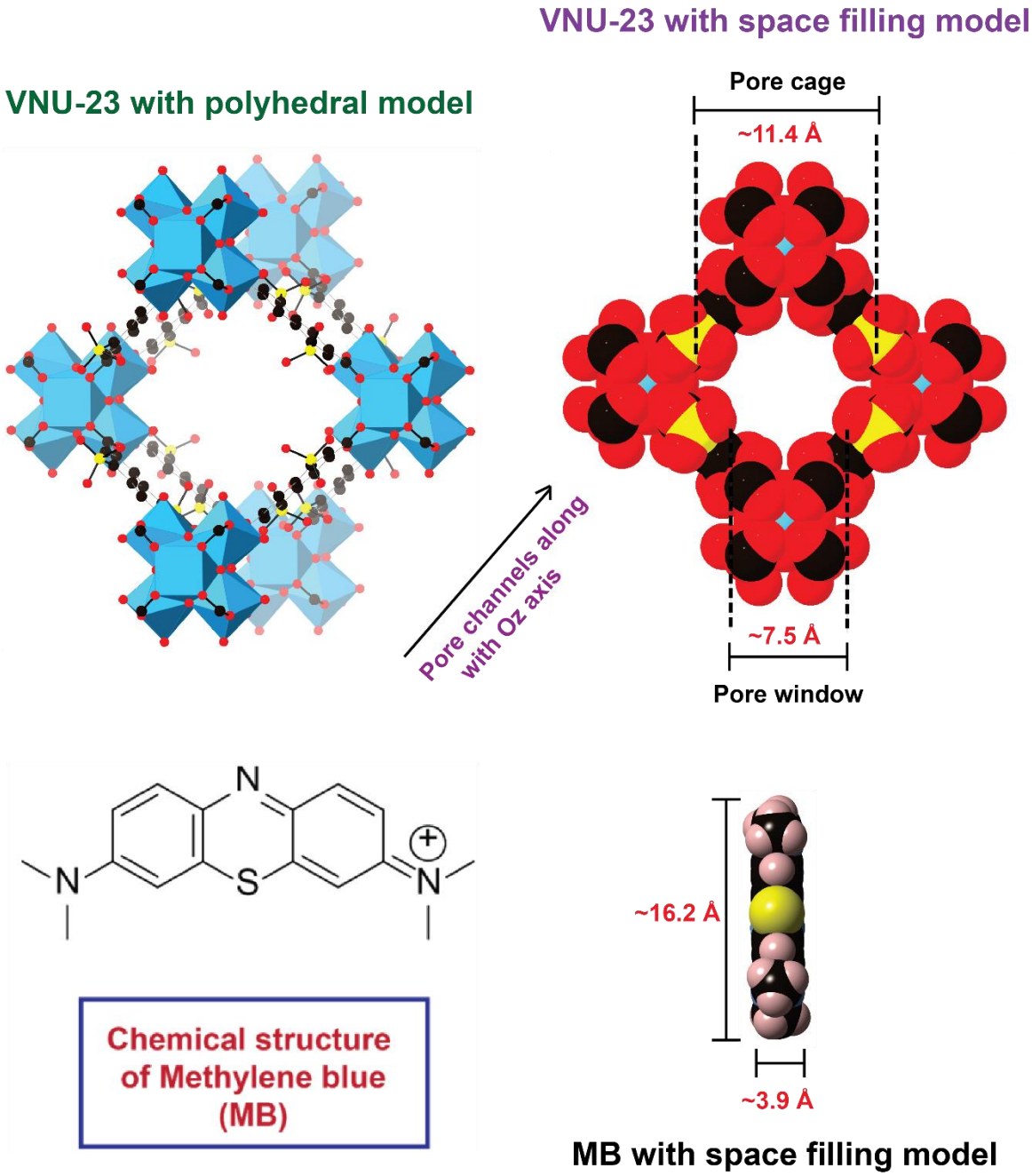


**Figure S1.** The structure of VNU-23 viewing along with Oz axis. Atom colors: Zr, blue; C, black; S, yellow; O, red; all H atoms are omitted for clarity. The pore size of the material is measured in the CrystalMarker software. The mentioned pore sizes are corresponding with pore size distribution analysis (see in Fig. S15).

**Section S3.** $^{1}$H-NMR analysis of $H_3SNDC$ and $H_4SNDC$ linker

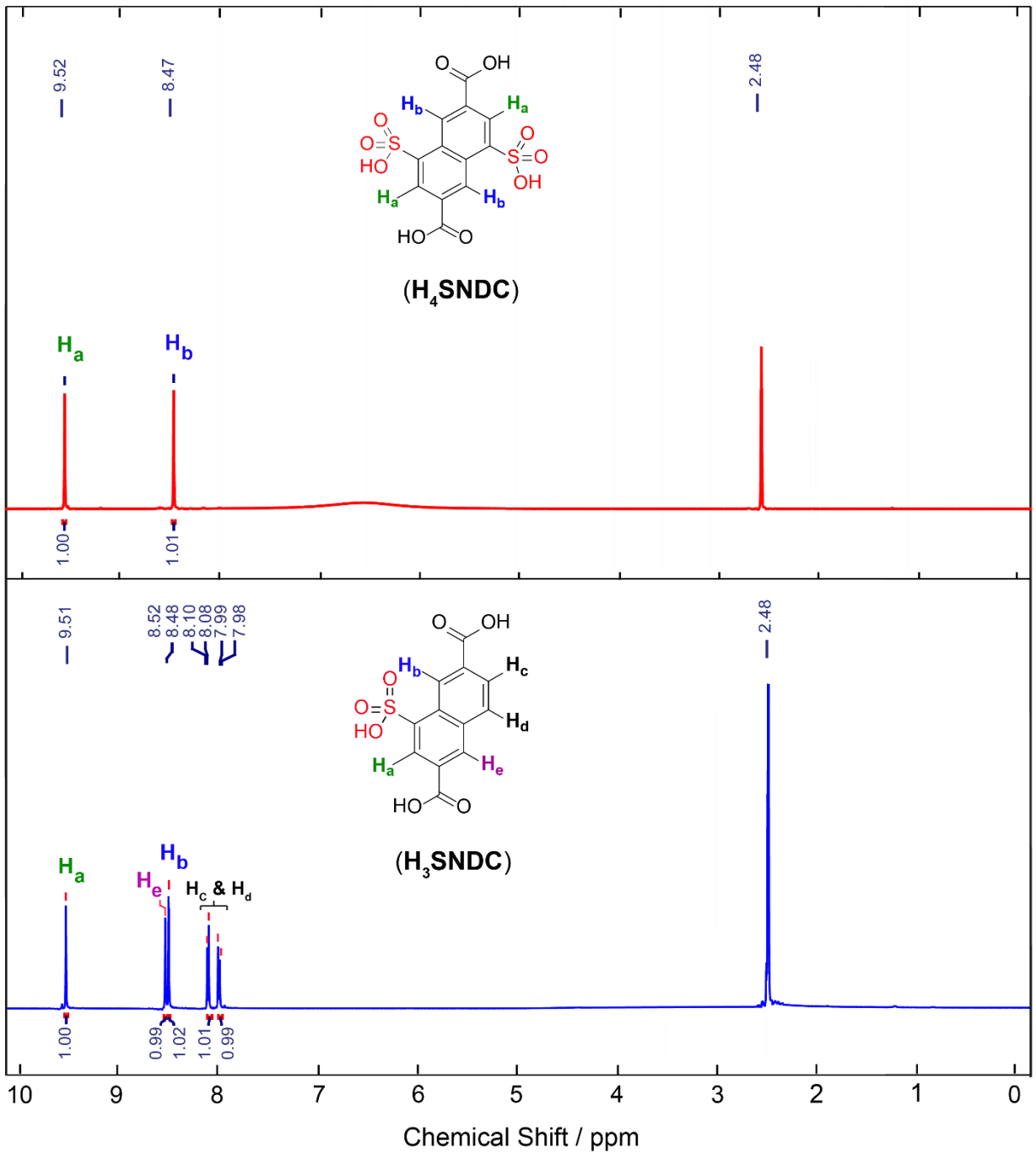


**Figure S2.** $^{1}$H-NMR analysis of the $H_3SNDC$ (blue) and $H_4SNDC$ (red) linker.

**Section S4.** The standard curves of MB and MO with different concentrations

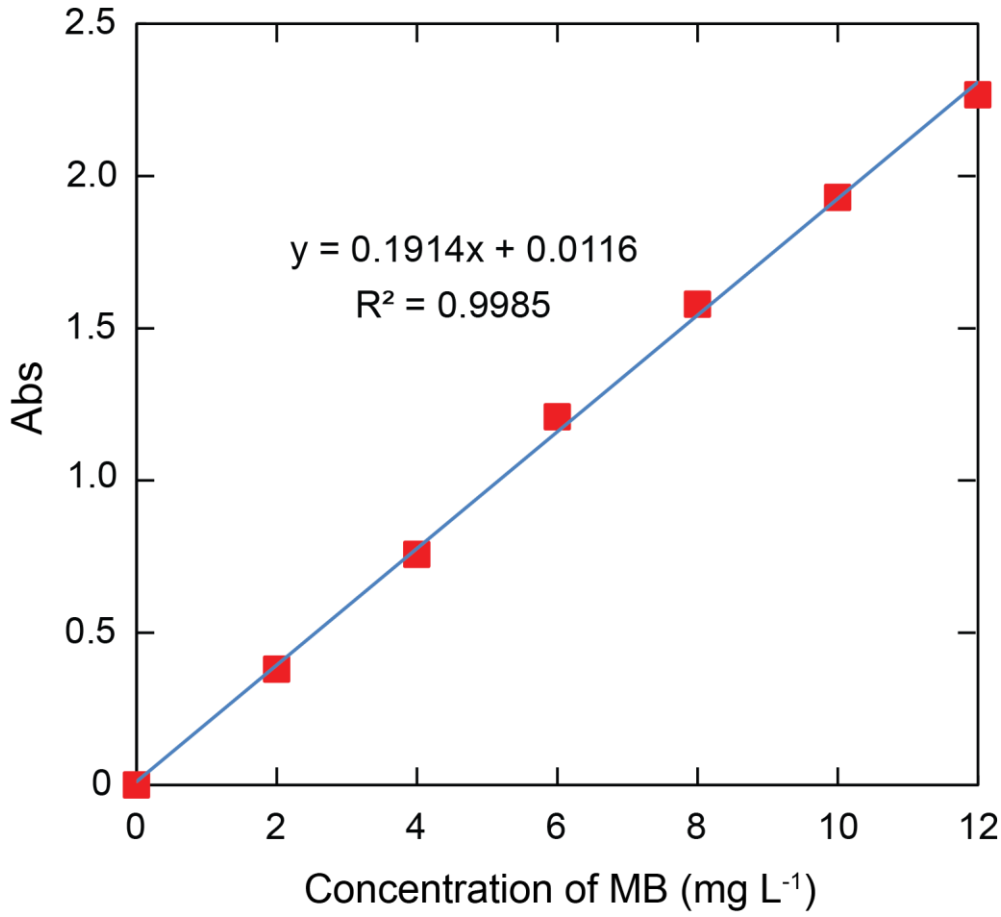


**Figure S3.** The relationship between the absorbed intensity (red dots) of MB and different concentrations of 0 - 12 mg $L^{-1}$ by linear fitting.

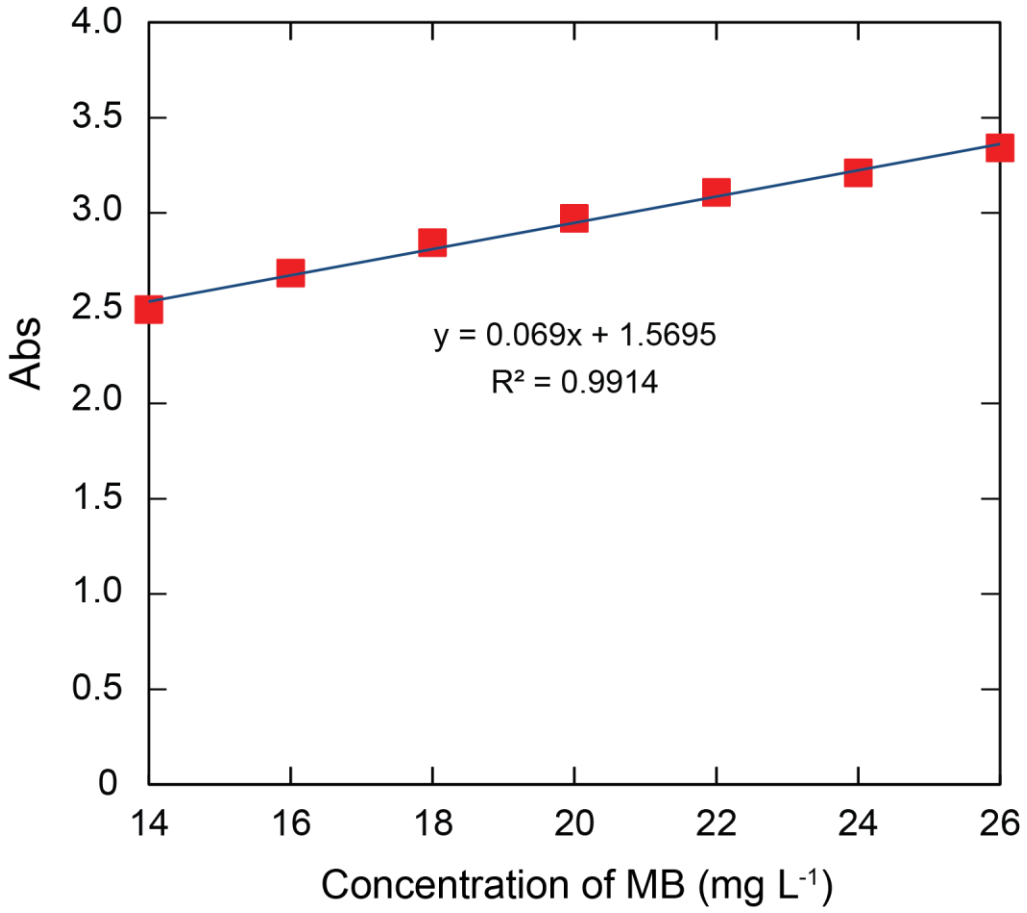


**Figure S4.** The relationship between the absorbed intensity (red dots) of MB and different concentrations of 14 - 26 mg $L^{-1}$ by linear fitting.

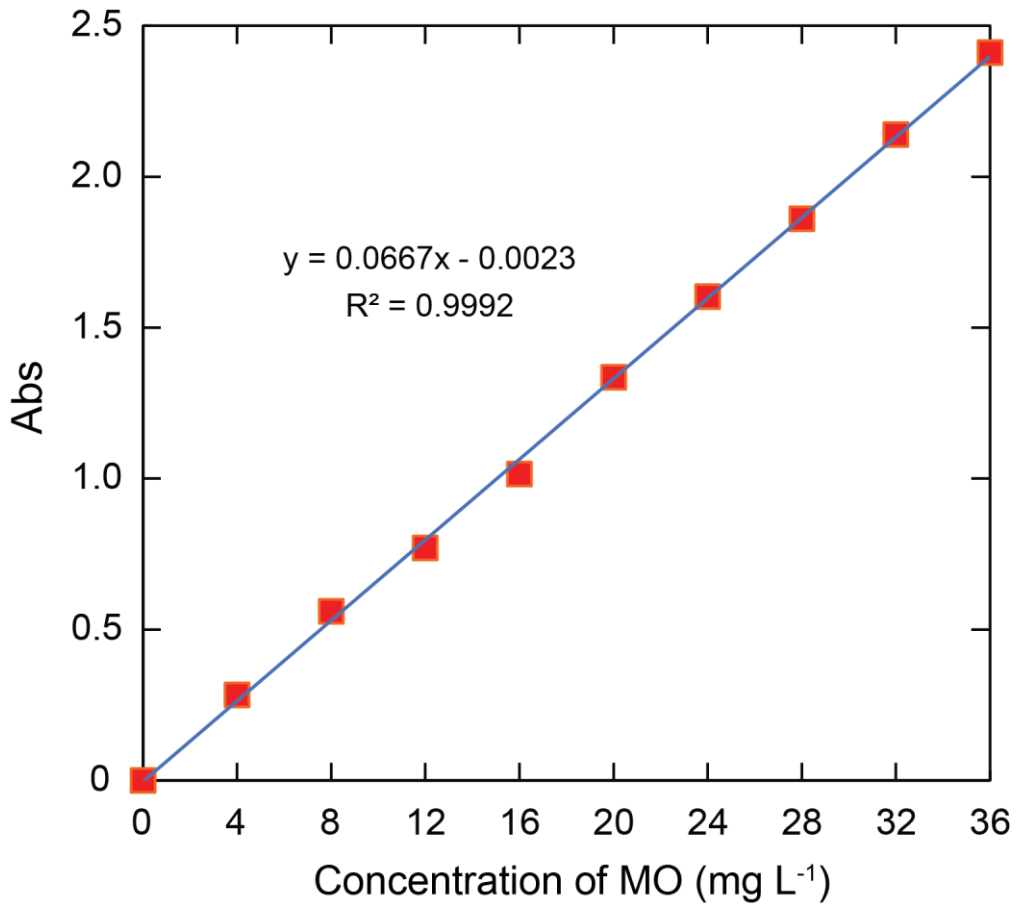


**Figure S5.** The relationship between the absorbed intensity (red dots) of MO and different concentrations of 0 - 36 mg $L^{-1}$ by linear fitting.

**Section S5.** Fourier Transform Infrared (FT-IR) analysis

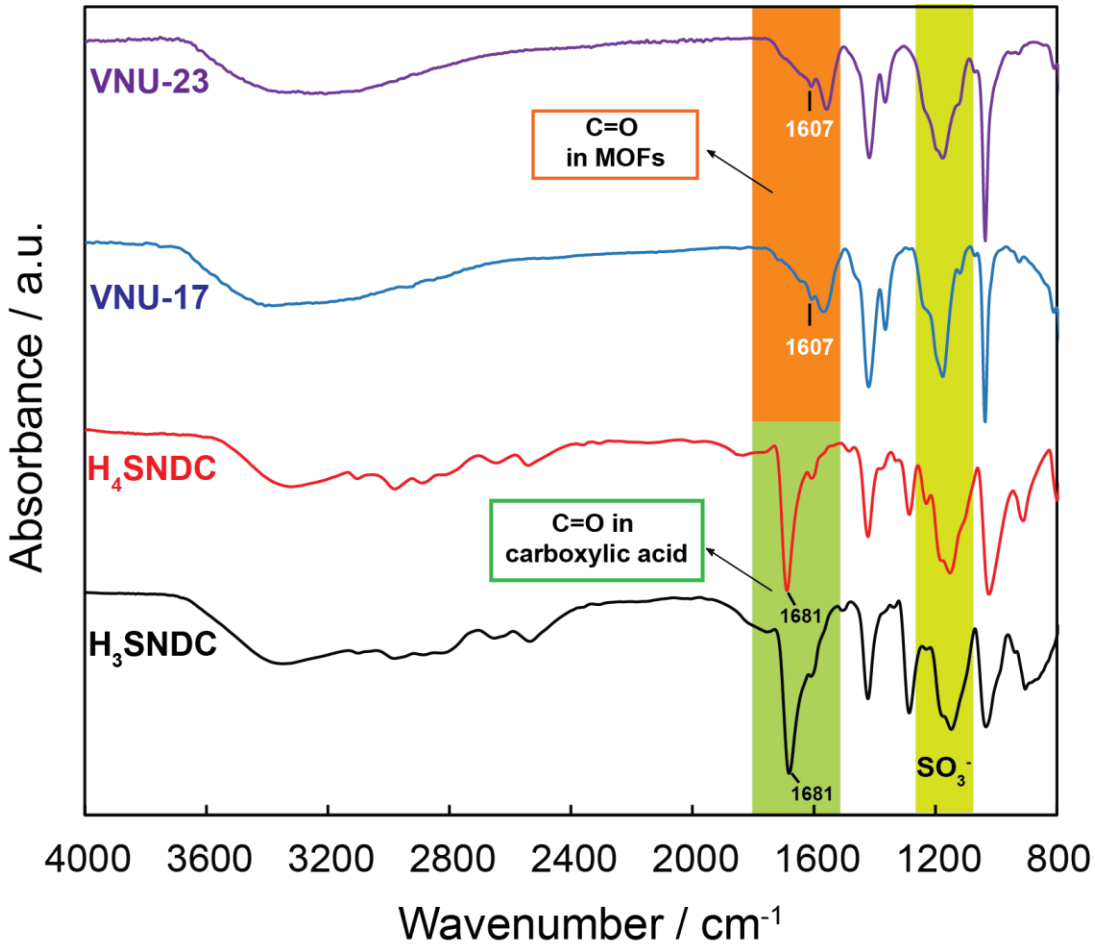


**Figure S6.** FT-IR spectrum of $H_3$SNDC (black) and $H_4$SNDC (red) linker in comparison with VNU-17 (blue) and VNU-23 (purple) materials.

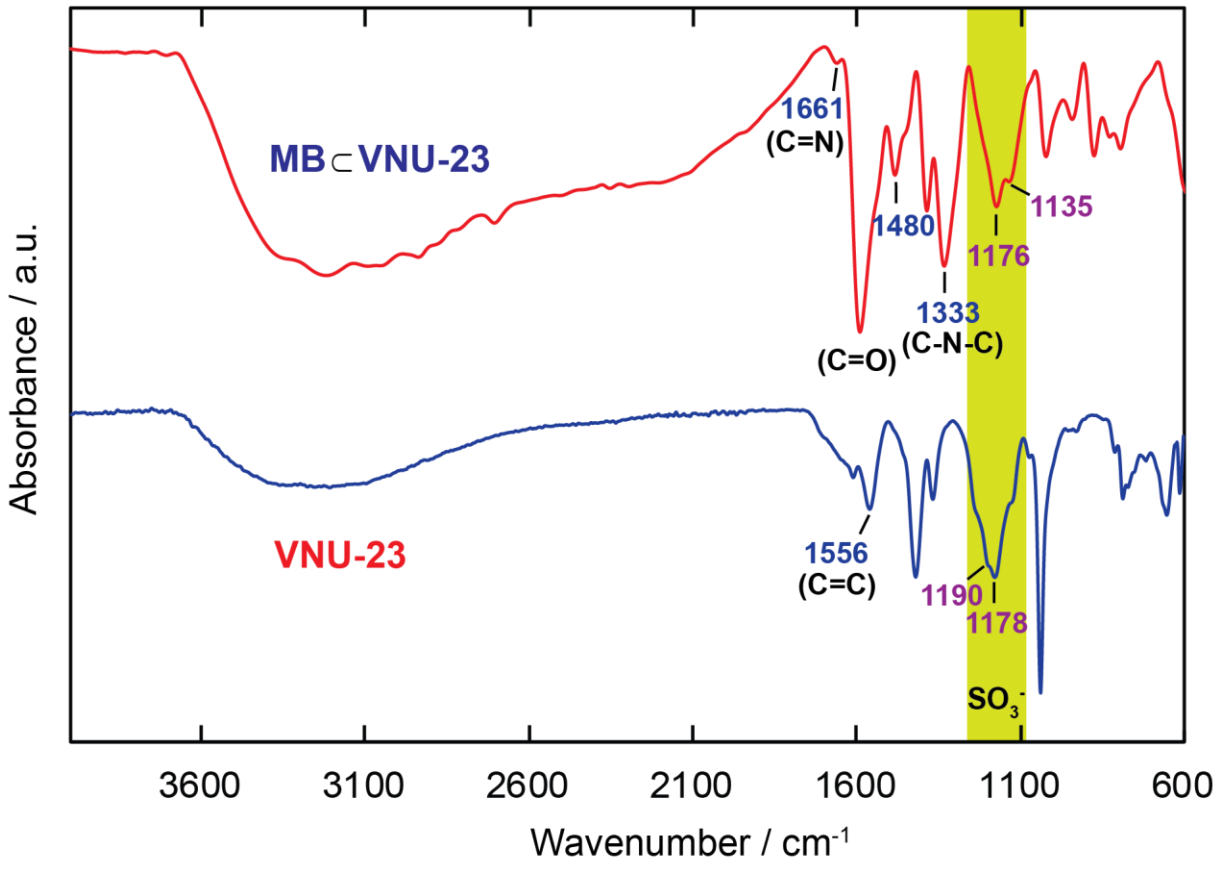


**Figure S7.** FT-IR spectrum of VNU-23 (blue) in comparison with VNU-23 after adsorption of MB (MB⊂VNU-23) (red).

**Section S6.** Powder X-ray Diffraction Patterns (PXRD)

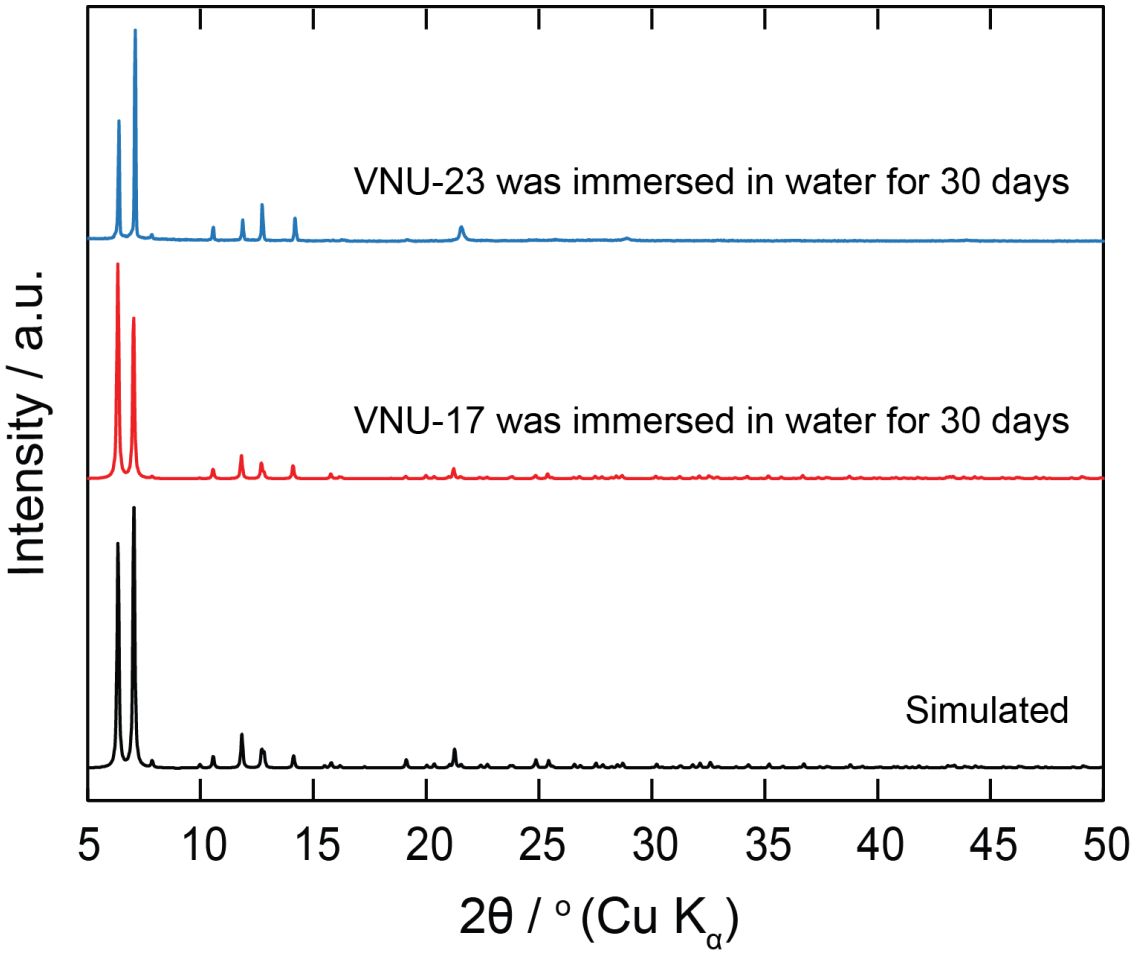


**Figure S8.** PXRD patterns of simulated structure (black) in comparison with VNU-17 (red) and VNU-23 (blue) immersed in water for 30 days.

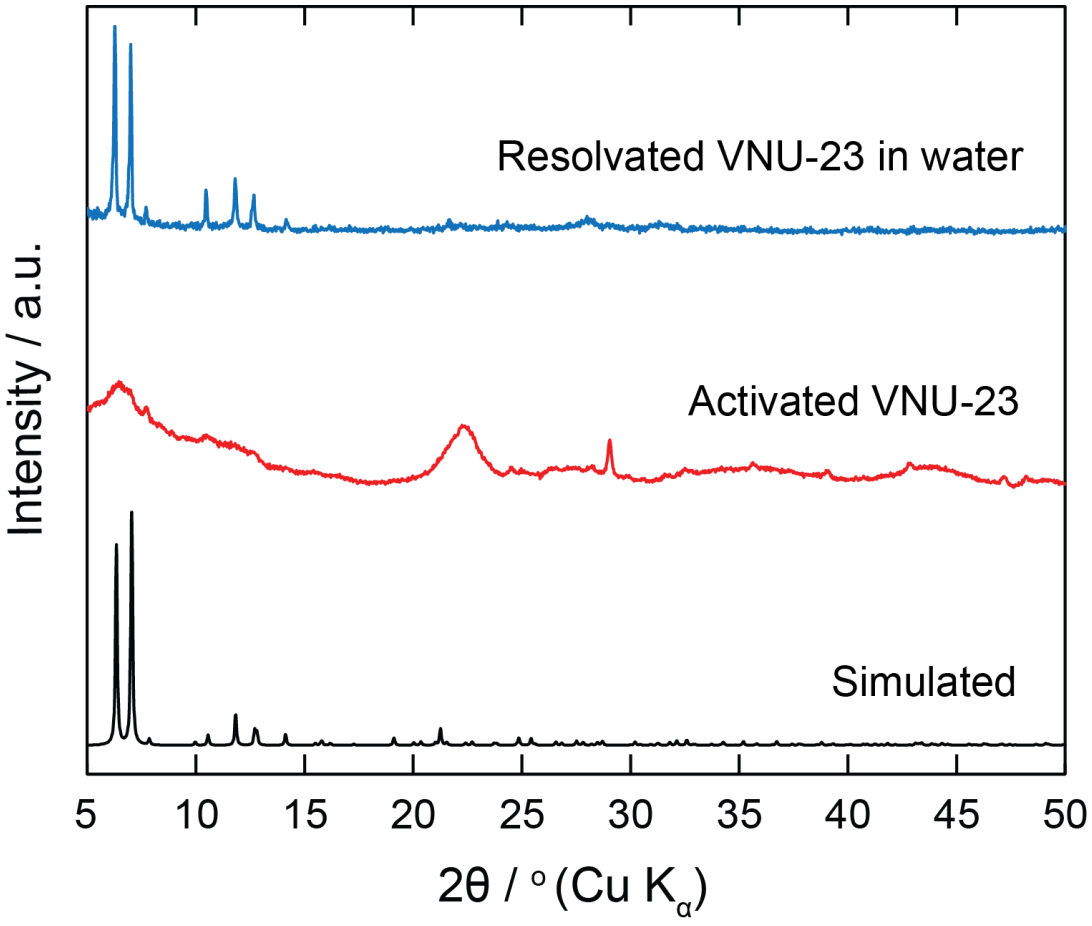


**Figure S9.** PXRD patterns of simulated VNU23 (black) in comparison with activated VNU-23 (red) and resolvated VNU-23 in water (blue).

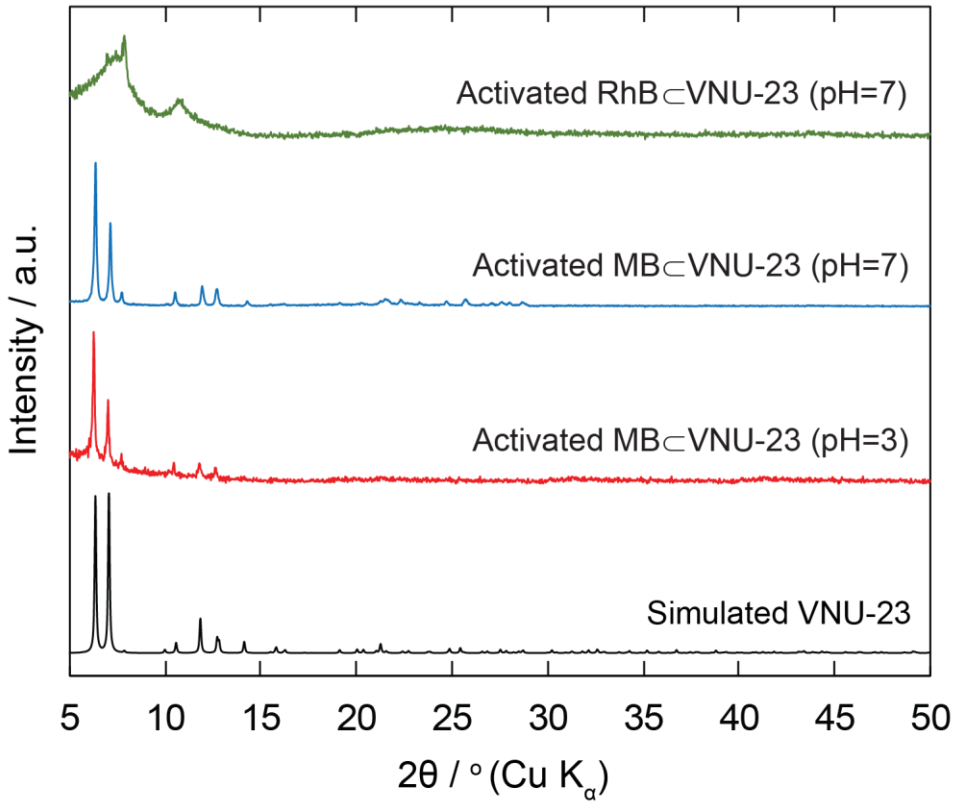


**Figure S10.** PXRD patterns of simulated VNU23 (black) in comparison with activated MB⊂VNU-23 at pH = 3 (red), activated MB⊂VNU-23 at pH = 7 (blue) and activated RhB⊂VNU-23 at pH = 7 (green).

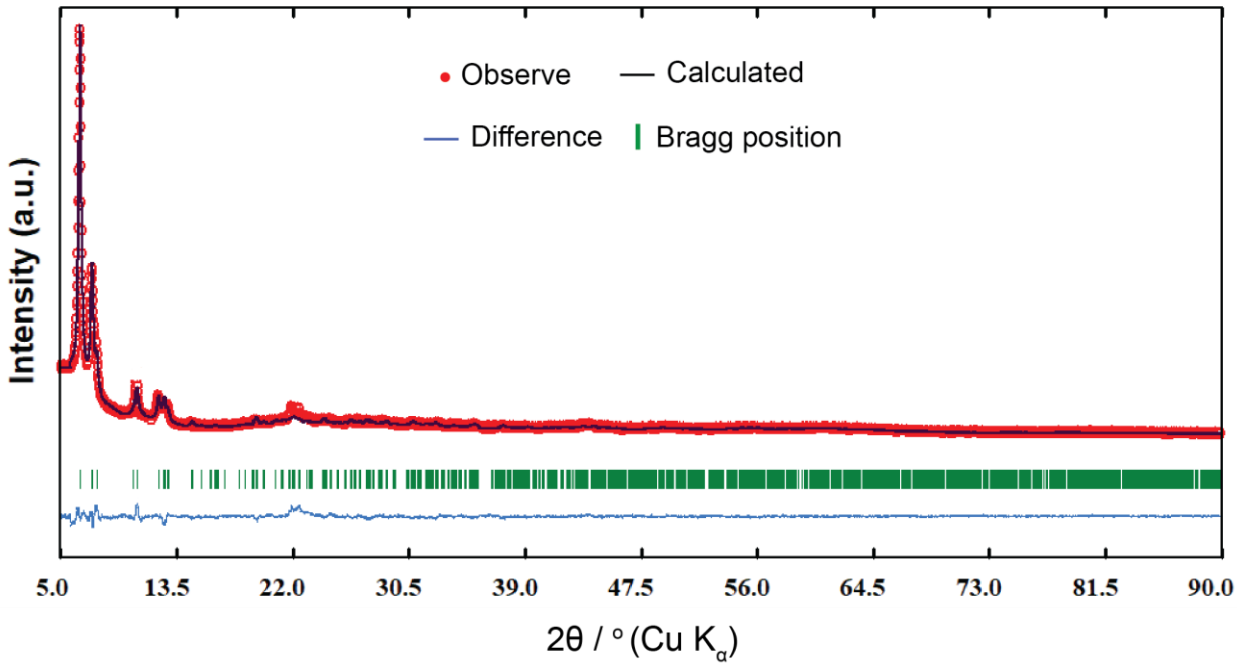


**Figure S11.** The Rietveld refinements using space group of MB⊂VNU-23 at pH = 7: The observe (red), calculated (black), and difference (blue) patterns. The Bragg positions are marked as green bars.

**Section S7.** Thermogravimetric Analysis (TGA)

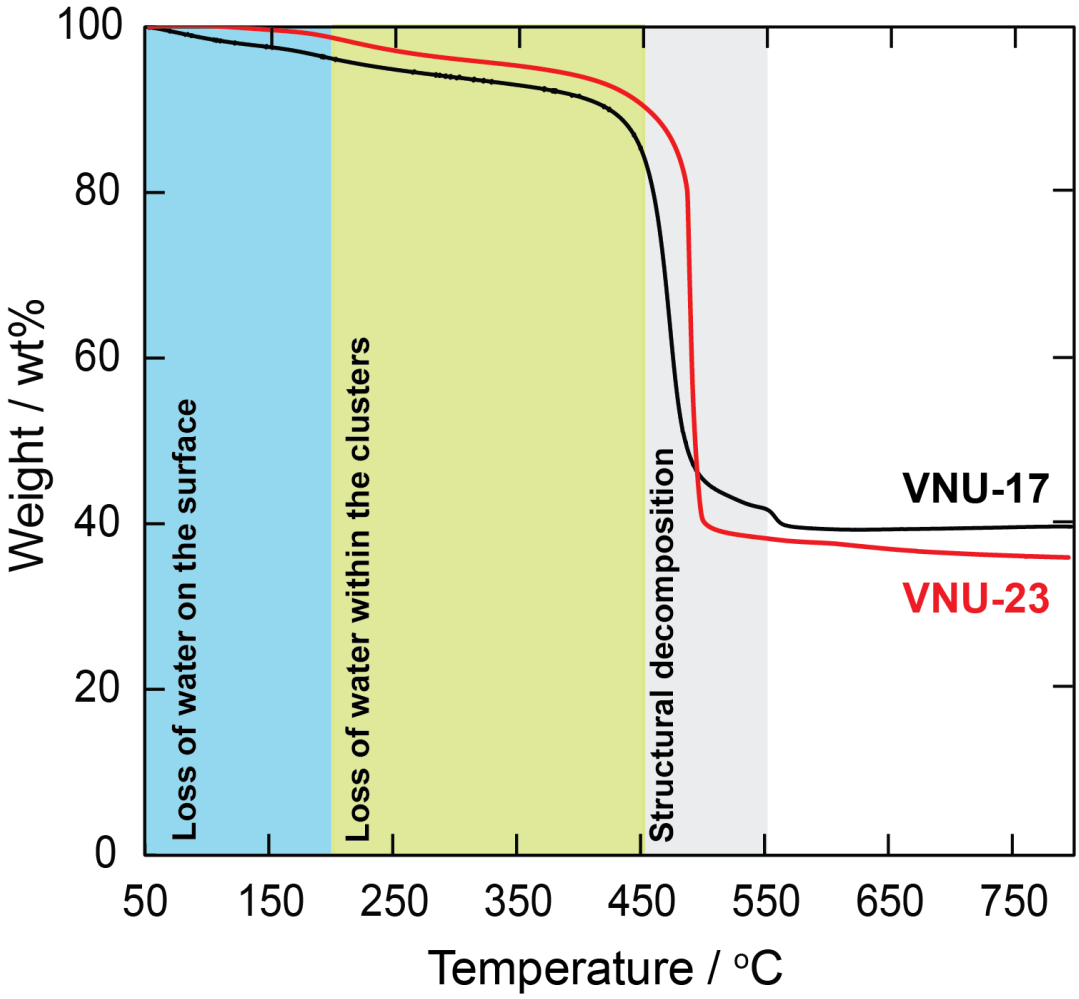


**Figure S12.** TGA curve of VNU-17 (black) and VNU-23 (red).

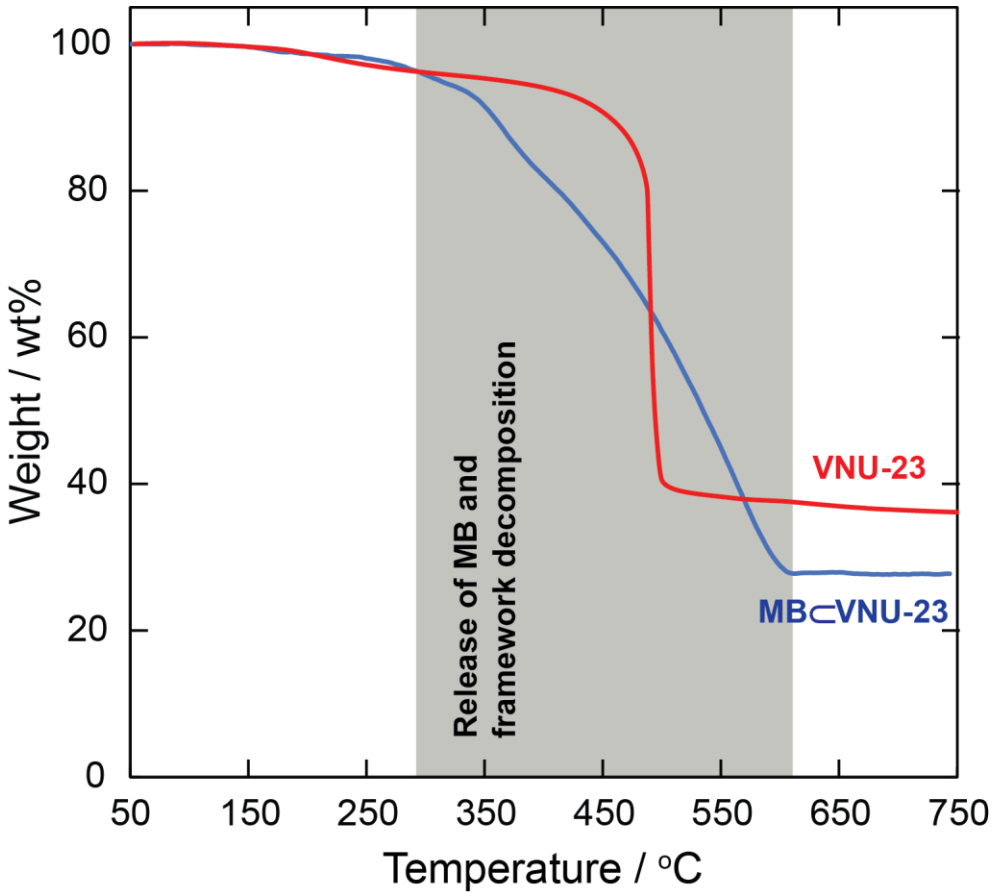


**Figure S13.** TGA analysis of VNU-23 (red) in comparison with MB⊂VNU-23 (blue).

## **Section S8.** $N_2$ adsorption and desorption isotherm

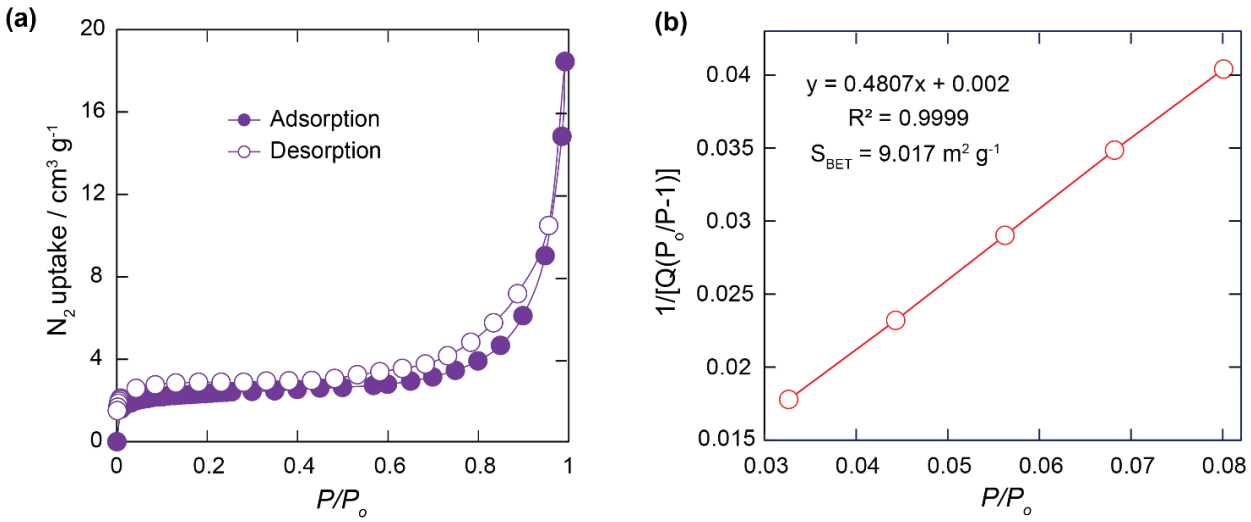


**(c)**

| $P/P_o$ range | 0.0327 - 0.0801 |
|---|---|
| Correlation Coefficient | 0.9999 |
| C | 239.665 |
| $Q_m$ ($cm^3\ g^{-1}$ STP) | 2.0716 |
| Molecular cross-sectional area (S / $nm^2$) | 0.1620 |
| BET surface area ($m^2\ g^{-1}$) | 9.017 |

$$S_{BET} = \frac{Q_m \times N_A \times S}{V}$$

Where $S_{BET}$ and $Q_m$ are the BET surface area and quantity adsorbed. $N_A$ is Avogrado's number, S is the molecular-sectional area and V symbolizes the molar volume of adsorbed gas.

**Figure S14.** $N_2$ adsorption-desorption isotherm of VNU-23 (a), Plot of the linear region of the adsorption $N_2$ isotherm used for the BET equation (b), summary of parameters in the BET analysis (c).

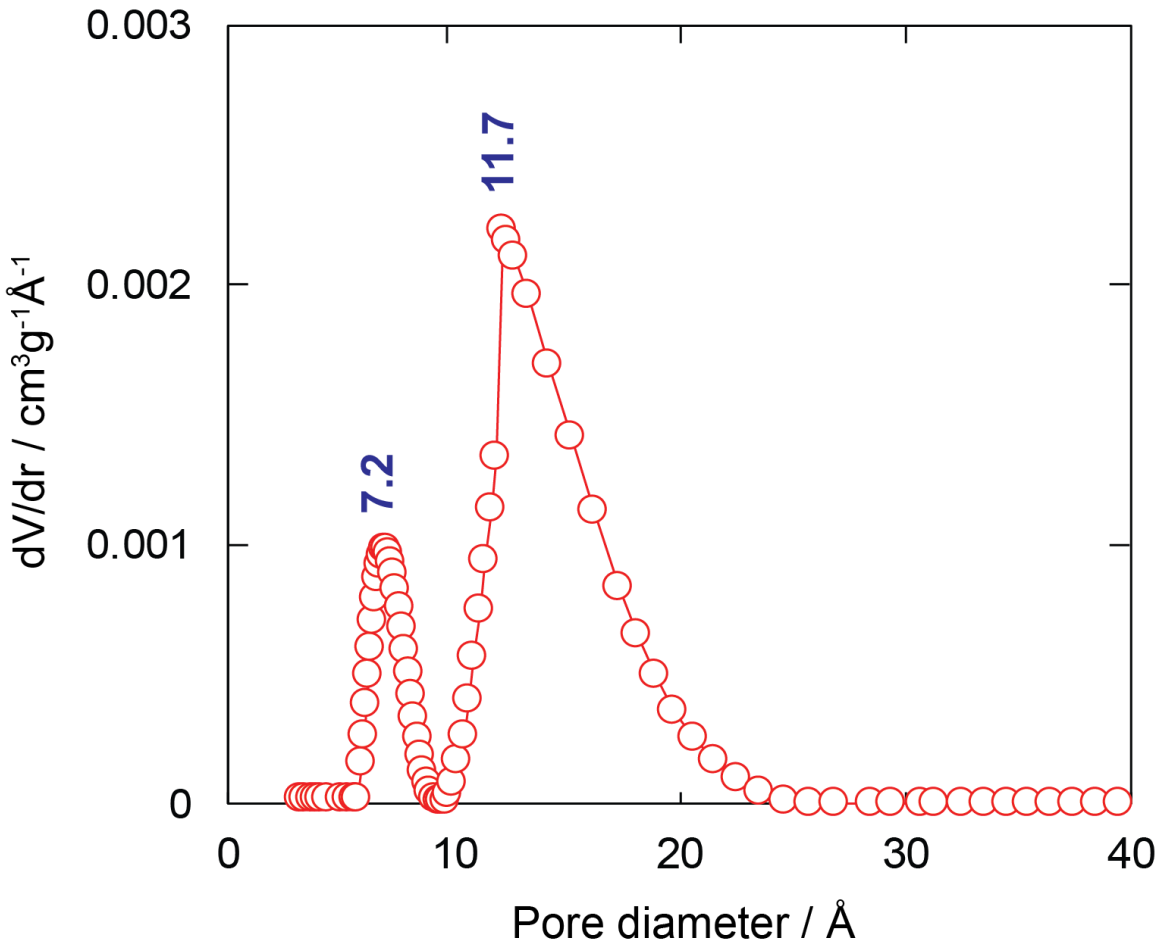


**Figure S15.** Pore size distribution of VNU-23. $N_2$ isotherm was analyzed by solid DFT implementing a hybrid kernel for 77K $N_2$ adsorption based on a carbon model containing slit pores. The estimated pore width around 7.2 and 11.7 Å should be corresponded window and cage pore, respectively.

## **Section S9.** Adsorption experiments

### The adsorption of MB onto VNU-17.

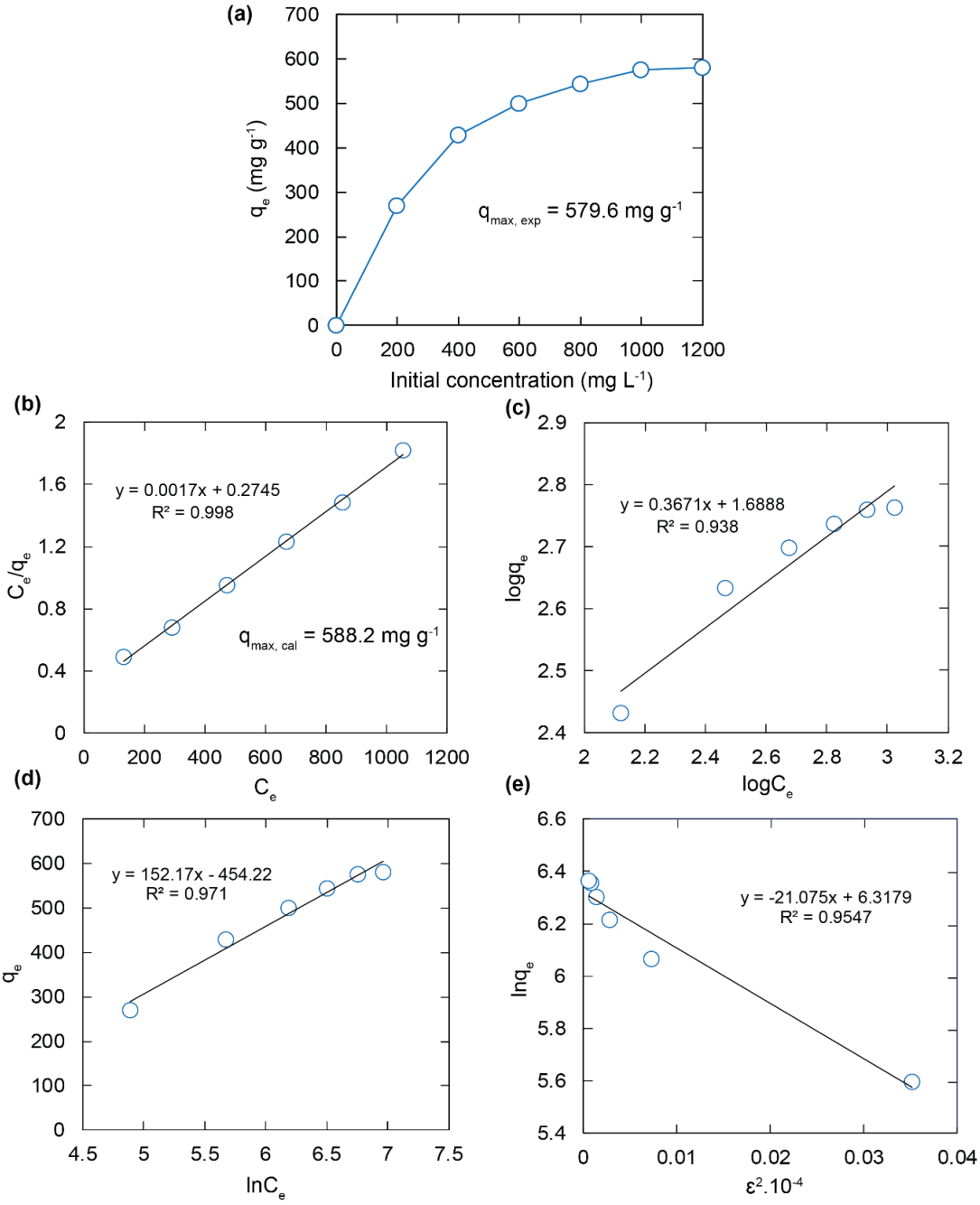


**Figure S16**. Effect of initial concentration on the adsorption capacity of MB onto VNU-17 [m = 20 mg, $V_{MB}$ = 100 mL, $C_o$: 200 - 1200 mg $L^{-1}$, pH = 7, t = 24 h] (a). Data fitting with the adsorption isotherm models: Langmuir (b), Freundlich (c), Temkin (d), and Dubinin-Radushkevich (e).

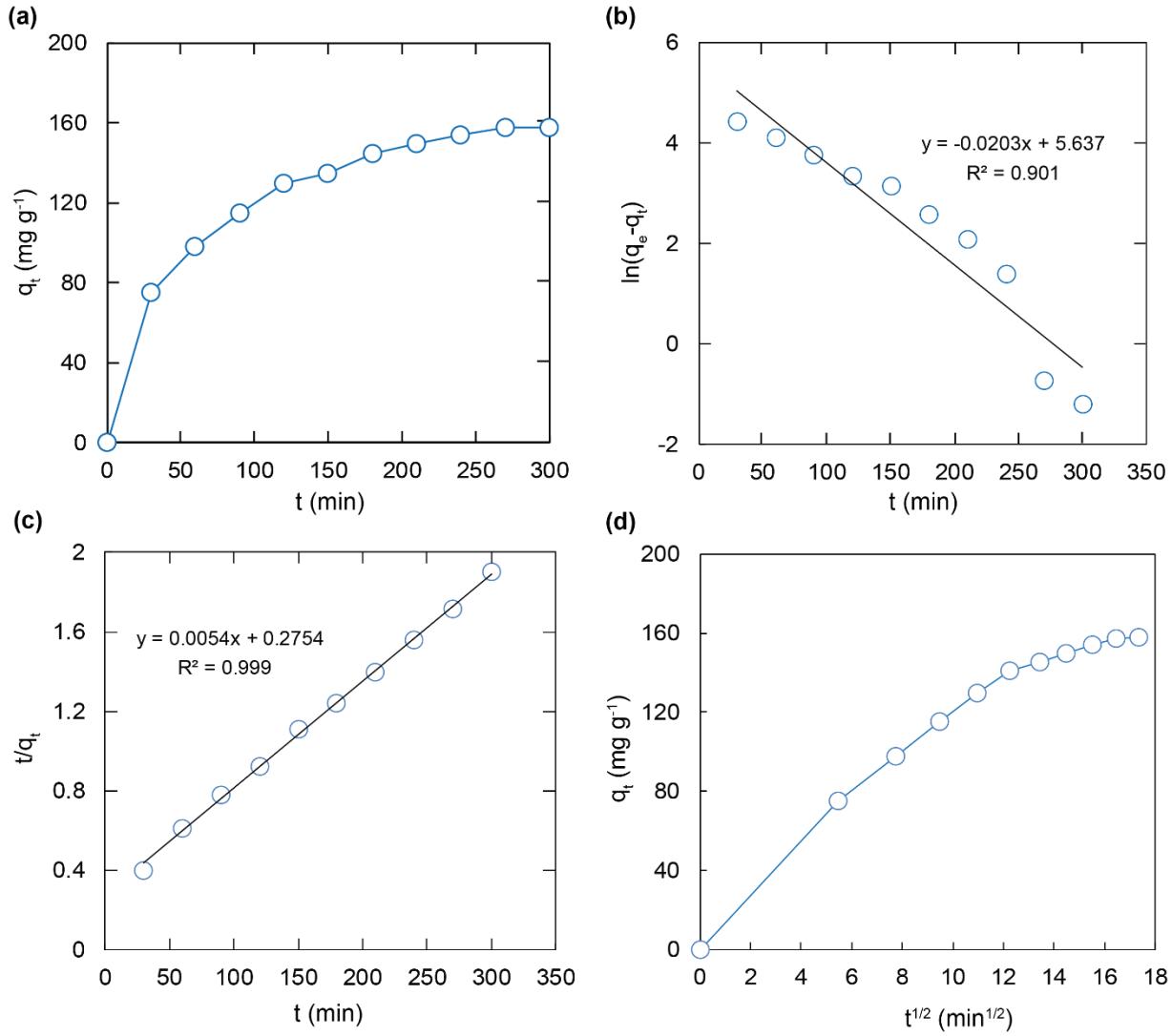


**Figure S17**. The kinetic curve for the adsorption of MB on VNU-17 [m = 5 mg, $V_{MB}$ = 20 mL, $C_o$ = 50 mg $L^{-1}$, pH = 7] (a). Data fitting with the adsorption models: pseudo first order (b), pseudo second order (c) and intra-particle diffusion model (d).

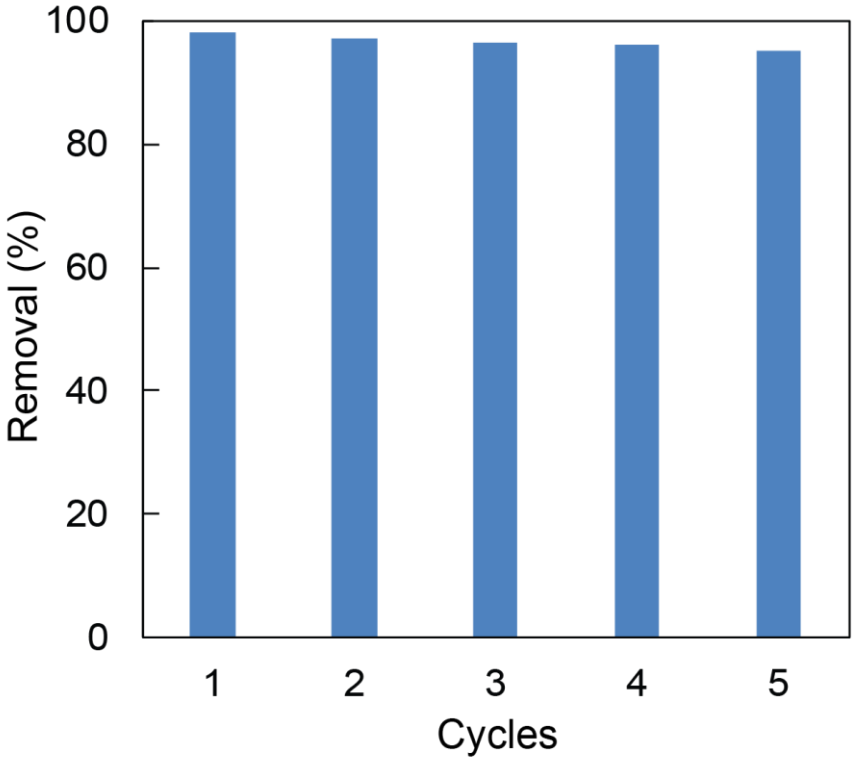


**Figure S18**. The reusability of VNU-17 in the adsorption process of MB. A removal efficiency of 95% is retained after five cycles.

**Temkin and Dubinin-Radushkevich (DR) isotherm of the adsorption of MB onto VNU-23.**

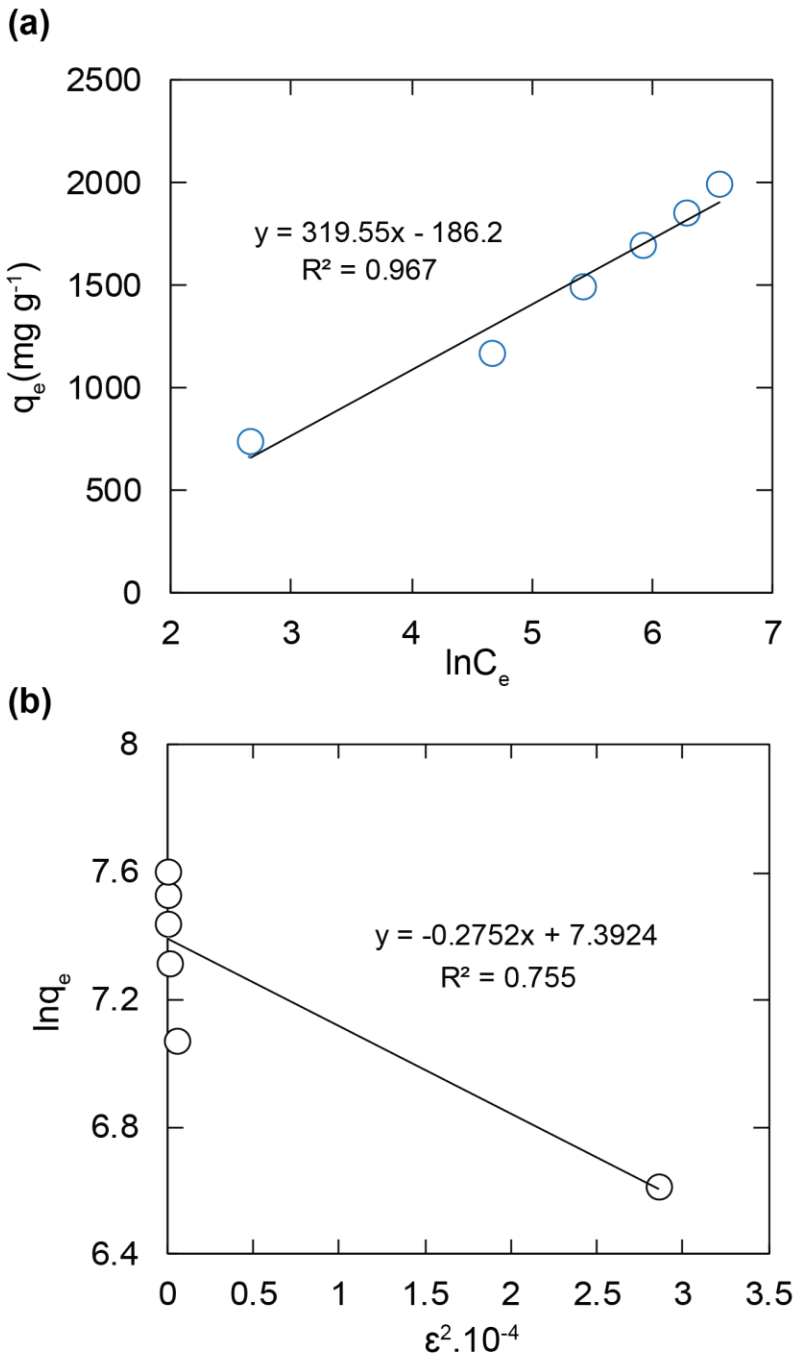


**Figure S19**. Data fitting with the adsorption isotherm models of MB onto VNU-23: Temkin (a), and Dubinin-Radushkevich (b).

**Section S10.** The stability of VNU-23 during the adsorption and desorption process of MB

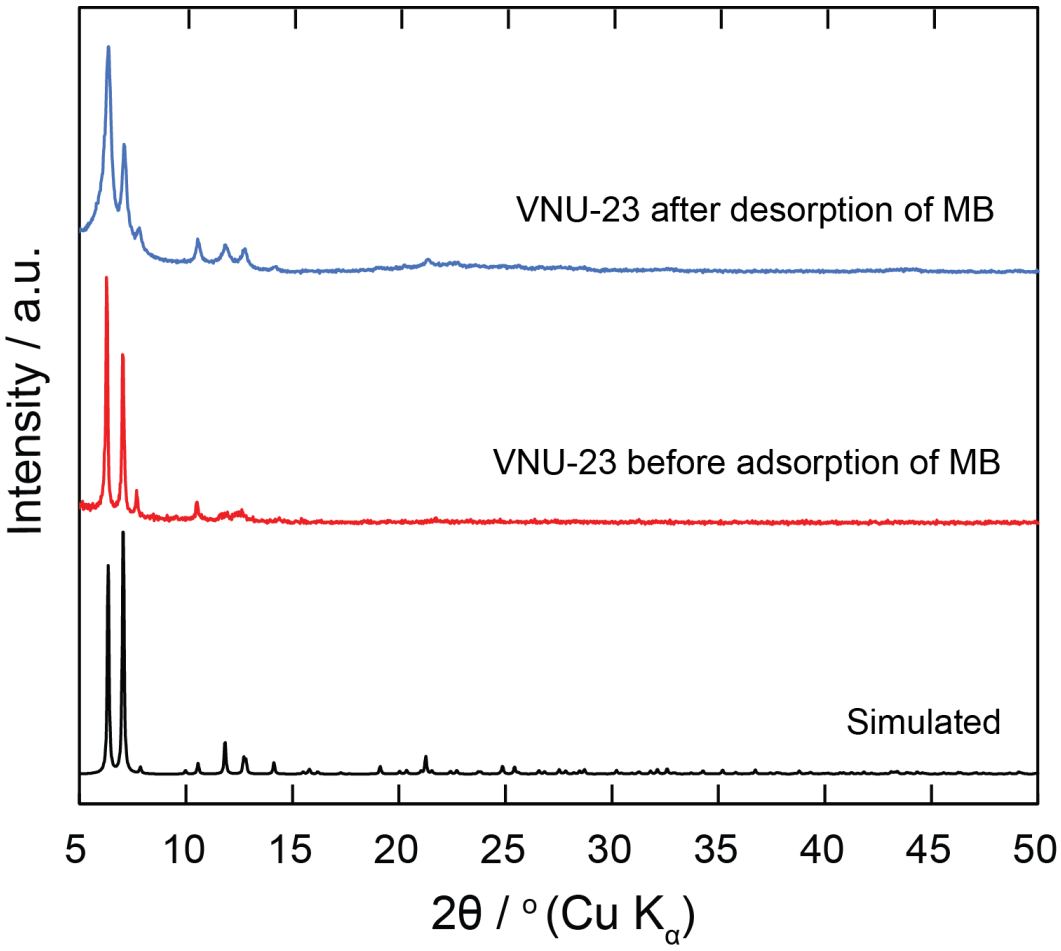


**Figure S20.** Simulated PXRD pattern of VNU23 (black) and VNU-23 before adsorption of MB (red) as compared to the the experimental pattern from the subjecting VNU-23 after desorption of MB (blue).

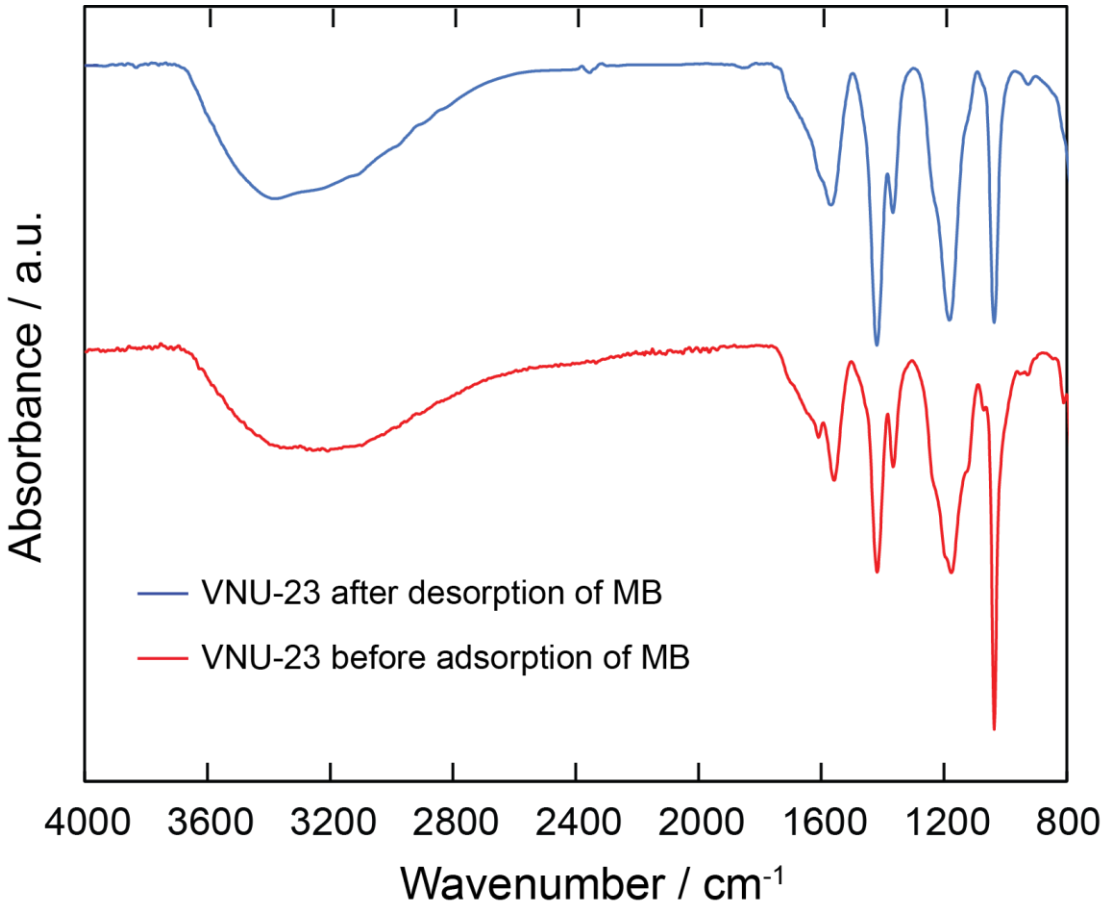


**Figure S21.** FT-IR spectrum of VNU-23 before adsorption of MB (red) as compared to the FT-IR spectrum of VNU-23 after desorption of MB (blue)